X-ray absorption in atomic iodine in the *K*-edge region

J. Padežnik Gomilšek,[1] I. Arčon,[2,3] S. de Panfilis,[4,5] and A. Kodre[6,3]
[1]*Faculty of Mechanical Engineering, University of Maribor, Smetanova 17, SI-2000 Maribor, Slovenia*
[2]*University of Nova Gorica, Vipavska 13, P.O. Box 301, SI-5001 Nova Gorica, Slovenia*
[3]*J. Stefan Institute, Jamova 39, P.O. Box 3000, SI-1001 Ljubljana, Slovenia*
[4]*Centro Studi e Ricerche "Enrico Fermi," Via Panisperna 89/A, 00184 Roma, Italy*
[5]*Research Center SOFT INFM-CNR, Universita di Roma "La Sapienza" Piazzale Aldo Moro 2, 00185 Roma, Italy*
[6]*Faculty of Mathematics and Physics, University of Ljubljana, Jadranska 19, SI-1000 Ljubljana, Slovenia*
(Received 30 November 2008; published 20 March 2009)

X-ray atomic absorption of iodine in the energy region of the *K* edge is determined from the absorption of iodine vapor at temperatures up to 1000 °C with appreciable dissociation of the molecular species. Kinetics of dissociation, relevant for isolation of the absorption of the atomic species, is discussed. The atomic signal is obtained as a linear combination of the highest-temperature absorption spectra at two vapor densities; the coefficients of the combination are determined from extended x-ray absorption fine structure (EXAFS) analysis of the molecular signal. Photoexcitation channels are identified in the *K*-edge profile and in the spectral features originating from multielectron excitations. The applicability of the atomic absorption as the true absorption background for EXAFS analysis is demonstrated.

DOI: 10.1103/PhysRevA.79.032514 PACS number(s): 32.30.Rj, 32.80.Aa, 78.70.Dm

I. INTRODUCTION

Excited states of an atomic system can be prepared in a number of ways. Photoelectric excitation is probably the cleanest among them since the reaction channels are effectively pruned off by selection rules. Hence the apparent simplicity of an atomic absorption spectrum, with a smooth monotonic decrease in the absorption coefficient over long stretches of photon energy and sudden sharp absorption edges, due to the strong prevalence of photoionization channels leading into just a few singly ionized states, well separated in energy. The simple picture, however, shows a wealth of detail when examined in a high-resolution, high-sensitivity measurement, whereby also the weak reaction channels can be studied. In addition to the complex shape of the absorption edges due to the contribution of the narrow resonant excitations, the smooth region of the spectrum above the edge is populated by tiny sharp features due to the multielectron photoexcitation (MPE) processes. The amplitude of an MPE channel depends sensitively on the electron correlation in the atomic system, and thus provides a fine test of theoretical models.

The MPE spectral features can be reliably studied only in atomic x-ray absorption, i.e., in absorption measured on a pure monatomic sample of an element. The above-edge spectral region measured on dense elemental or compound samples is pervaded by oscillations of the strong x-ray absorption fine structure (XAFS) originated from scattering of the photoelectron on the atoms in close vicinity. The atomic absorption was studied on noble gases [1–4] and on predominantly monatomic vapors of some volatile metals [5–10]. The strong interest in MPE data has led to procedures whereby an approximate atomic absorption is extracted from the spectra of much more easily prepared dense samples by elimination of XAFS signal [11,12]. Although the results are useful for some purposes, only the absorption spectra of monatomic gases yield the atomic absorption in the full and exact sense, comprising only the intra-atomic effects in photoabsorption.

Monatomic samples of nonmetallic elements are more difficult to prepare, the vapors–with exception of noble gases–consist of strongly bound covalent molecules. However, iodine vapor can be thermally dissociated to an appreciable extent already at 1000 °C. X-ray absorption in elemental iodine has been thoroughly studied, mainly in solid and liquid phases, in large ranges of temperature and pressure. Along these studies and the studies of iodine ion in several solvents, Buontempo *et al.* [13] also measured the low-temperature vapor and extracted the basic structural data of the molecule. In addition, several groups of MPE were identified in the absorption spectrum beneath the molecular extended x-ray-absorption fine-structure (EXAFS) signal. The MPE outside the wider x-ray absorption near-edge structure region (XANES) have also been recognized in absorption spectra of dense iodine compounds, where the structural signal persisted only in a short spectral range above the *K* edge, due to a strong disorder or extremely large distance to the first neighbors with non-negligible photoelectron scattering power [14,15].

In the present study, we have exploited thermal dissociation of iodine vapor to determine the atomic absorption of the element. The feasibility of the procedure had been tested in an earlier measurement [16]: from a series of absorption spectra of the vapor between 250 and 1000 °C, the EXAFS signal of the iodine molecule was removed, and a clear, albeit rather noisy, atomic absorption spectrum of iodine has been extracted. The result has led to the present optimized experiment in which a direct way of separation of the molecular and atomic absorption has been devised. An independent part of the study, the absolute determination of the x-ray absorption coefficient in a wider region of the *K* edge, has already been published [17] (henceforth referred to as Sec. I-A).

 ©2009 The American Physical Society

II. CHEMICAL KINETICS

The data on iodine dissociation on which to plan the experiment are very scarce: some isolated data points can be found as, e.g., 1% dissociation at 575 °C and 1 atm [18]. There is no simple formula to predict the degree of dissociation at a given vapor density and temperature in this apparently simple chemical process. A deeper consideration shows that indeed there is no simple equilibrium which could be described by the above three variables. While the dissociation takes place mainly in the gas by molecular collisions, the recombination runs efficiently only at a solid surface, whence the molecules diffuse into the gas. The density and degree of dissociation thus change with the distance from the walls, and the quality of the walls has a pronounced effect. For the case of weak dissociation, the equation governing the density of molecules ρ in a stationary state can be linearized to

$$D\nabla^2\rho - k\rho = 0, \tag{1}$$

where D is the diffusion coefficient in the gas and k is the rate of collisional dissociation. The recombination is described by a boundary condition of a constant influx. For cylindrical geometry (a long tube) the radial dependence of the density can be written as

$$\rho = \rho_0 I_0\left(r\sqrt{\frac{k}{D}}\right), \tag{2}$$

where I_0 denotes the modified Bessel function. The density at the axis ρ_0 is given by the recombination efficiency of the wall. A similar equation can be written for the density of the atomic species. At the axis where the gas is probed by the x-ray beam, the degree of dissociation α can still be described locally by the chemical kinetics,

$$\frac{\alpha^2}{1-\alpha} = \kappa\rho_{\text{tot}}e^{-E/kT}, \tag{3}$$

with E in the Boltzmann factor representing the threshold energy for the dissociation, κ is the constant of the reaction $I_2 \leftrightarrow 2I$, and ρ_{tot} is the total iodine density.

While the effect of the temperature and density can be estimated from this relation, the degree of dissociation depends also on the unknown κ. In the pilot experiment with absorption cells of ~1 cm diameter, 13% dissociation was achieved at 1000 °C, the maximum accessible temperature in the present oven design.

III. EXPERIMENT

The measurement was performed at the BM 29 station [19] of ESRF, Grenoble, using a tunnel oven for temperatures up to 1000 °C, with independent temperature control of the central and the end segments [19,20]. The station was equipped with a Si 311 two-crystal monochromator with full width at half maximum (FWHM) resolution 3.9 eV. The intensity of the monochromatized beam was monitored with three ionization detectors, filled with krypton to the pressure of 0.2, 1, and 1 bar, respectively, and with addition of He to the total pressure of 2 bar. Absorption cells were placed between the first pair of detectors, and the reference absorption samples between the posterior pair.

Iodine absorption cells with the length of ~30 cm and the volume of ~138 cm^3 were made of fused quartz, with 0.25 mm quartz windows. The cells were filled with different amounts of elemental iodine (Merck, p.A. 99.5%,) to provide a range of vapor densities within a factor of 3, with the range of attenuation factors above the K edge between 0.5 and 1.6.

A cell was placed in the oven and aligned in the beam with the help of a fluorescent screen behind the cell. Initially, a scan of the energy interval of interest was performed on the absorption cell at room temperature, with solid iodine out of the reach of the beam. In this way, the attenuation of the beam in the cell windows and in the air along the beam path was determined. Subsequently, the cell was slowly heated to 240 °C, while monitoring the absorption of the beam. The saturation of the absorption showed that the element was completely vaporized. Several energy scans of the absorption in the vapor were performed, to serve as checks of reproducibility of the experiment and to improve the signal-to-noise ratio, at the initial temperature and at elevated temperatures up to 950 °C.

The absorption was measured in the interval from −300 to 1400 eV relative to the iodine K edge in steps of 0.5 eV in the region up to 200 eV above the edge and in steps of 3 eV further on. The energy scale of the monochromator was carefully calibrated to the energy of the Xe K edge, relying on the Heidenhain absolute angle encoder. In full detail, the energy calibration is described in Sec. I-A.

IV. ABSORPTION SPECTRA OF IODINE VAPOR

The measured absorption spectrum at any temperature is a combination of the atomic and molecular absorption. The latter comprises the structural (EXAFS) signal and, strictly speaking, also a particular molecular background, not entirely identical to the atomic absorption of the monatomic species. The differences arise mainly in double electron excitations involving transitions into unoccupied molecular valence orbitals [21–23]. The effects of nuclear motion, such as hot bands, conspicuous in optical spectra, remain unresolved within the lifetime width of the iodine 1s level.

Although the absorption spectra measured at different temperatures represent different linear combinations of the atomic and molecular component, the separation of the two is not entirely straightforward since the parameters of the structural signal, most notably the interatomic distance and the amplitude of the vibration, also change with temperature. The separation, as demonstrated in the pilot experiment [16], although cumbersome, is still feasible, but the result, obtained from the change in the absorption coefficient with temperature, tends to be burdened with excessive noise.

In the present study, however, a direct procedure is introduced exploiting the kinetics of the dissociation. The structural parameters of the EXAFS signal depend on the temperature, but not on the density of the gas. The absorption spectra measured on absorption cells with different vapor density at the same temperature are independent linear com-

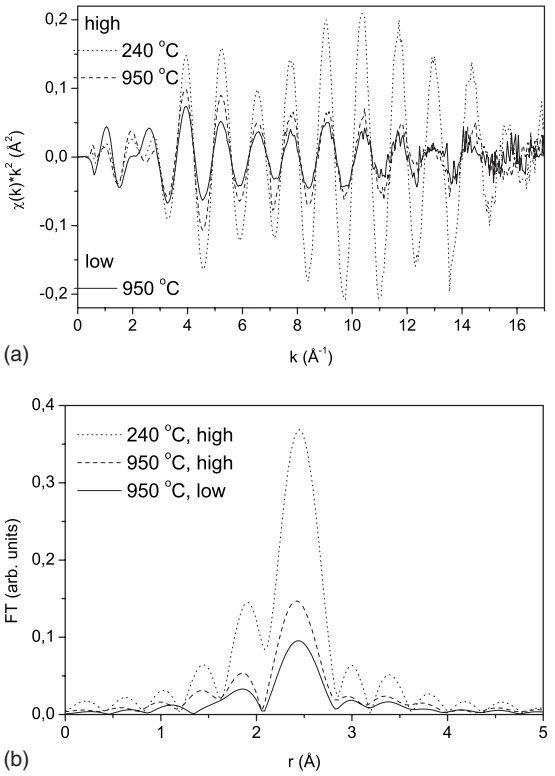

FIG. 1. The structural signal of the high-density and low-density molecular iodine vapor in (a) k and (b) R space. The decay of the signal with the temperature, caused by the increase of the Debye-Waller factor and the dissociation of the gas, is shown.

binations of exactly the same components. The coefficients of the combinations are given by the most straightforward parameters of the spectra: the amplitude of the structural signal is proportional to the density of the molecular component, while the total density of iodine is given by the magnitude of the absorption edge. Thus, the accuracy of the separation of the atomic absorption depends on the precise determination of the ratio of these two numbers for the spectra of the vapor at different temperatures and densities. In principle, it would be enough to measure and analyze two spectra at different vapor densities and the highest accessible temperature. Additional temperature points can be used to check the premises of the experiment: the low-temperature spectra, e.g., should exhibit pure molecular absorption.

The structural signal of the diatomic iodine molecule is sufficiently simple to allow a full theoretical reconstruction—at least in the harmonic approximation (Fig. 1). There is a single-scattering path of the photoelectron to be taken into account, with its four-leg echo just below the sensitivity threshold. The parameters of the path are related to the basic data on the I_2 molecule. The summation over vibrational modes gives the exact expression for the Debye-Waller factor $e^{-2\sigma^2 k^2}$ [24]:

$$\sigma^2 = \frac{\hbar^2}{M k_B T_E} \coth \frac{T_E}{2T}, \tag{4}$$

where σ denotes the mean-square relative displacement, M the mass of iodine atom, k_B is the Boltzmann's constant, T_E is the Einstein temperature, and T is the temperature of the vapor. Cubic terms in the expansion of the interatomic potential give rise to a linear change in the interatomic distance r_0 with temperature, $\sigma^{(1)} = a \cdot r_0 \cdot T$ and to a modification of the structural signal through the third cumulant $\sigma^{(3)}$ of the radial distribution function. However, these structural parameters are interrelated [25]:

$$\frac{\sigma^{(1)}\sigma^2}{\sigma^{(3)}} = \frac{1}{2 - (4/3)(\sigma_0^2/\sigma^2)^2}, \tag{5}$$

where σ_0^2 denotes zero-point contribution to σ^2. In the temperature range of the experiment, the right side of the relation approaches the high-temperature limit of 1/2. The common EXAFS model thus constrains the set of parameters to σ^2 from Eq. (4) with a single parameter T_E, $\sigma^{(3)}$ from Eq. (5), and constants a and r_0. Along with these, the model uses also intrinsic EXAFS parameters of E_0, the adjustment to the precise zero energy of the photoelectron, and the photoelectron coherence yield S_0^2, in the present case exploited to renormalize the molecular fraction in the vapor, setting it to 1 in the 240 °C spectrum.

TABLE I. Results of a simultaneous EXAFS modeling of the five spectra, r=2.0–3.0 Å, k=4–12 Å^{-1}, k weights 1, 2, and 3, Hanning window, r_0=2.66 Å. Uncertainties of the last digit are given in parentheses unless the parameter is fixed or derived.

Vapor density	High				Low
T (°C)	240	650	800	950	950
$N=1-\alpha$	1	0.97 (3)	0.93 (3)	0.84 (4)	0.54 (3)
r (Å)	2.668	2.670	2.671	2.672	2.672
σ^2 (Å^2)	0.0046	0.0079	0.0092	0.0105	0.0105
$\sigma^{(3)}$ (10^{-5} Å^3)	6.2	19	26	33	33
S_0^2			1.06 (3)		
E_0 (eV)			1.2 (3)		
a (10^{-6} K^{-1})			5 (1)		
T_E (K)			299 (4)		
r_{fit}			0.0028		

With this EXAFS model, the low-density spectrum at 950 °C together with high-density spectra at four temperature points 240, 650, 800, and 950 °C is analyzed in a single variational procedure, employing the above physical constraints on the model parameters. The high-density spectra with a better signal-to-noise ratio serve to improve the overall accuracy of results. The quality of the low-density spectrum limits the common k-space fitting range to 4–12 Å^{-1}. With the R range of 2–3 Å the fit uses 24 independent data points for the evaluation of 9 parameters. Variation with parallel k weighting values 1, 2, and 3, known to reduce the correlation between the model parameters is used.

The best-fit values of the parameters are listed in Table I, together with the derived physical parameters of the vapor. The low value of quality-of-the-fit measure r_{fit} indicates an extremely good agreement of the model and data. The value of T_E=299(4) K stands in a very good agreement with the value 306 K from uv measurements [26] ($kT_E = \hbar\omega$). Buon-

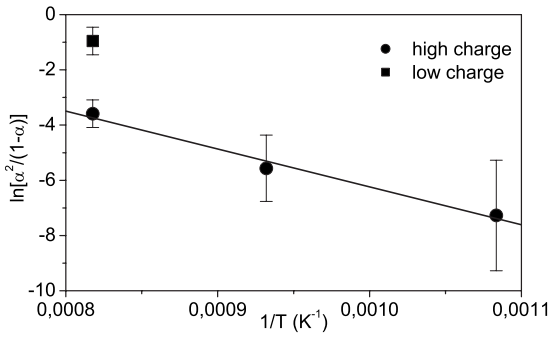

FIG. 2. The degree of dissociation of iodine, derived from measured absorption spectra, as a function of temperature in a conveniently linearized plot.

tempo *et al.* [13] report the same value. A check on the hypothesized chemical kinetics is shown in a graph of Eq. (3), conveniently transformed into a linear relationship (Fig. 2).

Evidently, the degree of dissociation reaches ~16% and ~46% in the high-density and the low-density vapor, respectively, sufficiently different to ensure a reliable separation of the atomic absorption.

At the end, a minor point needs to be clarified. In the initial step of the EXAFS analysis, the EXAFS signal needs to be extracted from the measured data. In the IFEFFIT package used in the analysis [27,28] this is routinely performed by removal of an approximative background, built as a spline from the nonstructural low-k Fourier components of the data. While the difference between the true and the spline background may be unimportant for the strong EXAFS signal of high-density spectra, it becomes critical in the low-density spectrum where the amplitudes of EXAFS and the background are comparable. However, the exact atomic background of iodine is precisely the goal of this study, so that the entire procedure described above is performed in two iterations, first with the spline approximation and then with the background derived from the data. Is there any possibility that the procedure would lead to a false end result? No, since the exact background is a component of the data, and the entire procedure is devised to determine only the coefficients of the linear combination of the measured spectra which yields the background. In any case, the background could be exactly removed from the data by performing the EXAFS analysis on subtracted pairs of spectra. As an independent check, the pair of 950 °C spectra has been analyzed in this way. A practically identical set of parameters has been obtained but with wider error bars due to the lower amplitude of the signal and weaker constraints.

V. ATOMIC ABSORPTION

The spectra of low-density and high-density vapor, when renormalized to a unit molecular signal by division with respective values of N in Table I, will subtract to a pure (unnormalized) atomic absorption. The normalized result, together with its complementary molecular component, is shown in Fig. 3.

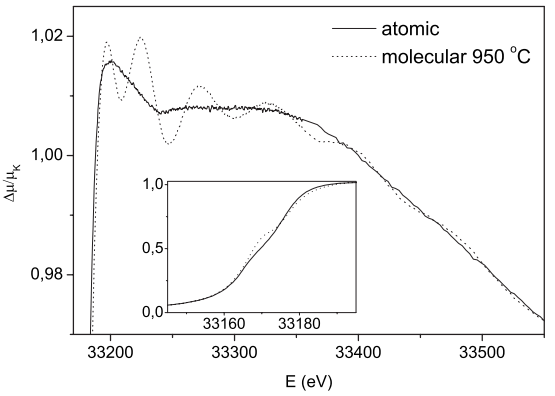

FIG. 3. The atomic and the molecular component in the iodine absorption (inset–edge profile).

As evident from the atomic edge profile, the large lifetime width of the K vacancy in iodine smears out a large part of the detail. One way to regain some of the resolution is the deconvolution after Filipponi [29]. The margins of the useful interval of the deconvolution, though, are rather close together. The emerging features are washed out if the width of the smoothing Gaussian is above 2.3 eV, and drowned in noise if it is below 1.9 eV. Within the sharpened edge a shelf is formed in the middle, showing the position of the pre-edge resonance [Fig. 4].

The feasibility of the deconvolution procedure also means that the hidden detail can be resolved by analytical modeling of the spectrum. Several models of the edge are built with a Lorentzian edge function $\arctan[2(E-E_K)/\Gamma]$, and one or two Lorentzian resonances, all convoluted with a Gaussian, modeling the instrumental width.

The simplest model is built of an edge and a resonance. In the fit, they are resolved 6 eV apart, significantly less than in self-consistent field calculations. The explanation is given by the principle introduced by Teodorescu [30]: the apparent position of the edge is given by the energy of the lowermost unresolved line in the Rydberg series. Our model resolves the first Rydberg line $[1s]5p$, and places the edge position at the energy of the $[1s]6p$ line. However, the resolved energy difference in the model is still far below the value of ~9 eV calculated in one-configuration Hartree-Fock (HF) [31] or Dirac-Fock (DF) [32] model. Conceivably, the configuration

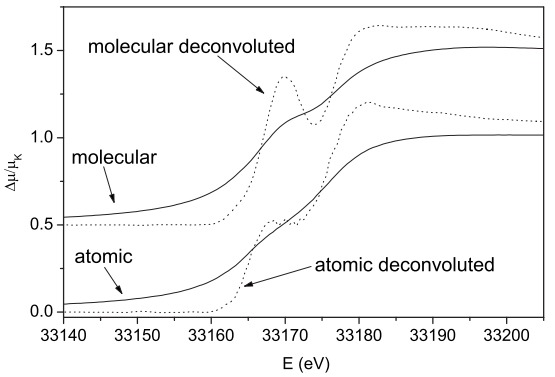

FIG. 4. Deconvoluted K-edge profiles of the atomic and molecular iodine at 950 °C.

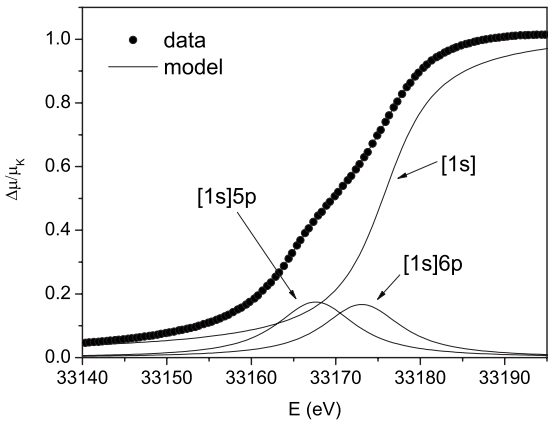

FIG. 5. The decomposition of the atomic iodine *K*-edge profile into contributions of single photoabsorption channels.

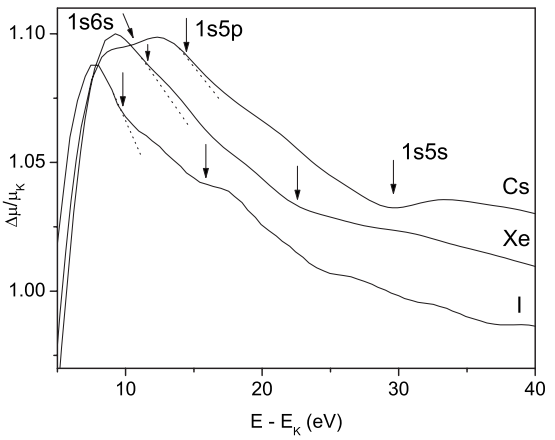

FIG. 6. Valence multielectron excitations in iodine and in the subsequent elements Xe and Cs, resolved in the deconvoluted data. The thresholds of $1s5p$ and $1s5s$ excitation groups are indicated by arrows.

mixing shifts the excited states with the promoted electron.

Introduction of another Lorentzian to model the $[1s]6p$ resonance weakens the robustness of the fit. A stable solution is obtained only with some constraints imposed on the parameters, of which a common value for the resonance widths seems the most reasonable. The edge energy is shifted to a higher energy. The amplitude of the newly introduced line is 0.96 of that of the first Lorentzian—a specific circumstance of iodine, where there is just one free orbital in the $5p$ subshell, against six in the completely empty $6p$ shell. The calculation of the oscillator strengths of the two resonances in HF and DF models yields the values 1.5 and 1.3, respectively, confirming the large amplitude of the second member of the Rydberg series. The reliability of the model is emphasized by the fact that the common width parameter stabilizes in the vicinity of the tabulated value of 10.6 eV [33] (Fig. 5).

Applying the same model to the edge profiles of the vapor spectra in the temperature series, the amplitude of the first resonance is seen to change appreciably, and there is a small shift of its position. The changes are proportional to the relative amount of the molecular species. In the pure molecular background, the amplitude of the $1s5p$ resonance is increased by 40%, and its energy by 1 eV, apparently due to the energy shift of the antibonding $^3\Sigma_u$ orbital. The absolute position of the edge E_K is discussed in detail in Sec. I-A.

VI. MULTIELECTRON EXCITATIONS

The results on the collective excitations in the atomic absorption spectrum, extracted either by deconvolution or by modeling, have little comparison either in theory or in earlier experimental data. The main way to judge their reliability is the comparison to the data on the neighbors. The comprehensive analysis of MPE in the *K* edge photoabsorption of Xe and Cs [7] includes a discussion of the theoretical aspects, namely, the specific mixing of configurations, indicated by the experimental data. Most of the conclusions, with exception of those involving Cs valence coexcitation $1s6s$ are also valid for iodine, due to the similarity of the internal structure of the atoms. For that reason, the present results will be given in relation to the Xe and Cs data. MPE in another closely related system, the iodine ion I^-, are discussed in a recent paper by D'Angelo *et al.* [15] where a table of corresponding excitation energies in Xe, I, and I^- is given.

The valence excitation $1s5p$ and $1s5s$ are, in view of the large lifetime width, incorporated into the profile of the absorption edge. The deconvolution reveals small humps on the high-energy side of the sharpened edge profile, the most pronounced of them at ~17 eV above the *K* threshold attributed to the $[1s5s]6s$ shake up and the subsequent shake off, while the stronger contribution of $[1s5p]$ group remains mainly hidden in the steeper stretch just before. The progression of the analogous excitation through the series I-Xe-Cs is clearly visible (Fig. 6). Parameters of individual excitation channels cannot be resolved for the lack of information on the spectral baseline formed by the main photoabsorption channel.

The subvalence excitations $1s4(d,p,s)$ are more amenable to analysis since an heuristic model [6] of the asymptotic regime of the postcollision interaction (PCI), modifying the photoabsorption immediately above the edge, can be applied. This is the exponential model of the PCI, with the exponential range constant adjusted to produce a strictly increasing residual of shake contributions of consecutive inner shells, as shown in Fig. 7. The range in iodine is estimated to 240 eV, close to Xe and Cs values of 260 and 280 eV, respectively.

With this exponential model, and exploiting the ansatz for the $4dps$ coexcitations, constructed for cases of Xe and Cs, three groups of coexcitations are resolved in iodine: in addition to the double excitations $1s4d$ and $1s4p$, the triple or even quadruple excitations of the $1s4d5p$ and $1s4d5p^2$ type. Separate ansatz elements are shown in Fig. 8(b): in addition to the Lorentzian resonances and edges, the exponential saturation $1-\exp[-\beta(E-E_{\text{th}})]$ as a model for the shake-off channel, with E_{th} the energy of the channel threshold. The characteristic span of the saturation $1/\beta$ is adjusted to 40% of the coexcitation energy $E_{\text{th}}-E_K$ as in [34]. The summed amplitude of all $1s4d$ shake channels is $(5.5\pm1.0)\%$ of the *K*-edge jump. The distribution into channel components is considerably less accurate. It is, however, supported by the quality and robustness of the fit and by the comparison with the Xe

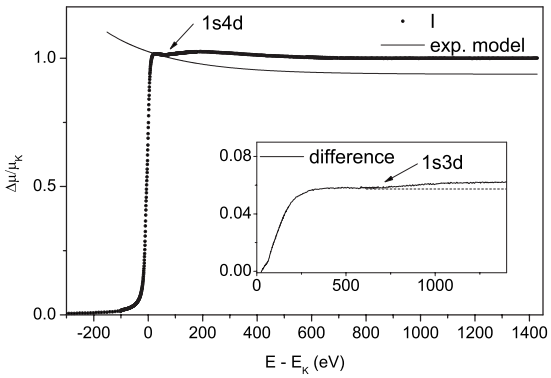

FIG. 7. The demonstration of the exponential model of PCI in iodine and its strictly increasing residual in the inset. The thresholds of $1s4d$ and $1s3d$ excitation groups are indicated by arrows.

and Cs case where the channels are better discerned.

The residual between the data and the $1s4(p,d)$ model in the inset of Fig. 7, in the form of a saturation profile with the threshold at ~700 eV (652 eV in Ref. [15]), can be attributed to $1s3d$ excitation. The extracted profile is, due to the high noise level, inferior in quality to the profiles in the earlier reports [13,14] and will not be analyzed in detail.

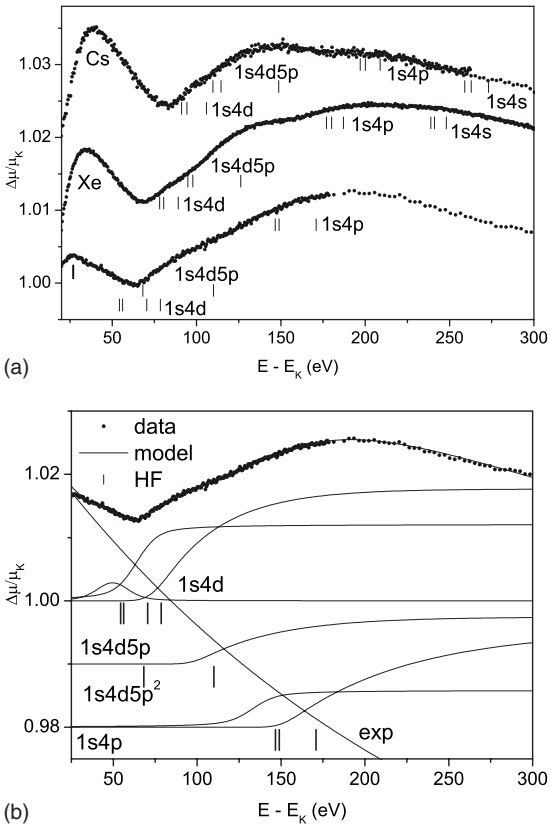

FIG. 8. The N-subshell coexcitations $1s4(d,p)$ in iodine. (a) comparison with Xe and Cs. Thresholds of resonance, shake-up and shake-off channels are indicated. (b) decomposition of the $1s4p,d$ spectral feature into contributions of individual channels, exp–the exponential model from Fig. 7. The spectra in both graphs are displaced along y axis for clarity.

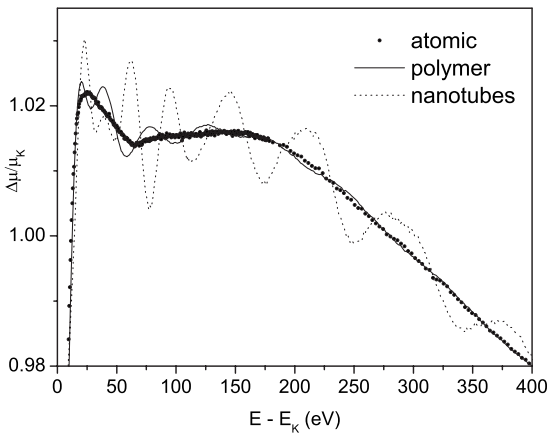

FIG. 9. Iodine atomic absorption as the natural absorption background for EXAFS spectra of iodine in organic polymer and in MoSI nanotubes.

VII. ATOMIC ABSORPTION BACKGROUND IN XAFS ANALYSIS

The atomic absorption of an element finds a practical application as the *atomic absorption background* (AAB) in XAFS analysis. Since MPE and XAFS effects occupy the same spectral region above an absorption edge, the XAFS signal need to be disentangled from the atomic absorption. The most widely used analysis routines such as IFEFFIT employ spline approximations, obtained from the separation of components in the k space with the assumption that the Fourier transform components above some minimal k (typically 1 $Å^{-1}$) arise predominantly from the structural signal, and those below from the long-wave distortions of the smooth monotonic absorption introduced by intra-atomic effects. The assumption may not be valid for samples with a weak XAFS signal, where the amplitude of structural Fourier components is suppressed to the size comparable to that of AAB. In such a case, only the removal of the exact atomic background yields the proper structural signal, and leads to reliable values of structure parameters in the subsequent XAFS analysis.

The application of iodine atomic absorption as AAB is demonstrated with independently measured iodine K-edge XAFS spectra of MoSI nanotubes [35] and of iodine-doped polymer of Ref. [14] (Fig. 9).

VIII. CONCLUSIONS

The atomic x-ray absorption of iodine, the basic data on an element, is determined in an experiment exploiting the low binding energy of the iodine molecule. It provides a direct comparison to the results of theoretical calculations, when available: in conjunction with the absolute absorption data presented in Sec. I-A it represents a most stringent test of the theory. Although some numerical manipulation of the experimental spectra has been performed, the atomic absorption is not reconstructed from the data on some molecular form of the element. The monatomic iodine is present in the absorption sample as a major constituent, and the numerical

handling to eliminate the contribution of the molecular species is limited to forming a linear combination of two directly measured spectra. There is no need for a model evaluation of any absorption contribution, not even of minor effects. The XAFS modeling of the experimental spectra is used only to determine a single coefficient, the mixing ratio of the two vapor constituents. Thus, the result is the exact atomic absorption in the full sense. Its application as the atomic absorption background in XAFS analysis is also demonstrated.

The information on the intra-atomic processes, the excitation energies and probabilities, to be extracted from the atomic absorption, is somewhat restricted by the large lifetime width of the iodine 1*s* vacancy. The results of the decomposition of the *K*-edge profile and of the strongest 1*s*4*d* group of excitation channels are entirely comparable to the results on the neighbor elements Xe and Cs. In the triad of consecutive elements, the trends in the MPE over a wider region of atomic number can be estimated.

ACKNOWLEDGMENTS

This work has been supported by the Slovenian Research Agency Research Program No. P1-0112. We acknowledge the European Synchrotron Radiation Facility for provision of synchrotron experimental facilities (proposal HD-156). We would like to thank Sakura Pascarelli and the technical staff of beamline BM29 for support at the experiment.

[1] J. M. Esteva, B. Gauthe, P. Dhez, and R. C. Karnatak, J. Phys. B **16**, L263 (1983).
[2] R. D. Deslattes, R. E. LaVilla, P. L. Cowan, and A. Henins, Phys. Rev. A **27**, 923 (1983).
[3] M. Deutsch and M. Hart, Phys. Rev. Lett. **57**, 1566 (1986).
[4] K. Zhang, E. A. Stern, J. J. Rehr, and F. Ellis, Phys. Rev. B **44**, 2030 (1991).
[5] J. P. Gomilšek, A. Kodre, I. Arcon, and R. Prešeren, Phys. Rev. A **64**, 022508 (2001).
[6] A. Kodre, I. Arcon, J. P. Gomilšek, R. Prešeren, and R. Frahm, J. Phys. B **35**, 3497 (2002).
[7] J. P. Gomilšek, A. Kodre, I. Arcon, and M. Hribar, Phys. Rev. A **68**, 042505 (2003).
[8] A. Mihelič, A. Kodre, I. Arčon, J. P. Gomilšek, and M. Borowski, Nucl. Instrum. Methods Phys. Res. B **196**, 194 (2002).
[9] A. Kodre, J. P. Gomilšek, A. Mihelič, and I. Arcon, Radiat. Phys. Chem. **75**, 188 (2006).
[10] A. Filipponi, L. Ottaviano, and T. A. Tyson, Phys. Rev. A **48**, 2098 (1993).
[11] J. P. Gomilšek, A. Kodre, I. Arcon, A. M. Loireau-Lozac'h, and S. Bénazeth, Phys. Rev. A **59**, 3078 (1999).
[12] G. Li, F. Bridges, and G. S. Brown, Phys. Rev. Lett. **68**, 1609 (1992).
[13] U. Buontempo, A. Di Cicco, A. Filipponi, M. Nardone, and P. Postorino, J. Chem. Phys. **107**, 5720 (1997).
[14] J. P. Gomilšek, I. Arčon, and A. Kodre, Acta Chim. Slov. **53**, 18 (2006).
[15] P. D'Angelo, A. Zitolo, V. Migliorati, and N. V. Pavel, Phys. Rev. B **78**, 144105 (2008).
[16] J. P. Gomilšek, A. Kodre, and I. Arčon, in *Proceedings of X05: X-ray and Inner-Shell Processes*, edited by C. T. Chantler (The University of Melbourne Press, Melbourne, 2005), p. 138.
[17] J. P. Gomilšek, I. Arčon, S. de Panfilis, and A. Kodre, J. Phys. B **41**, 025003 (2008).
[18] N. N. Greenwood and A. Earnshaw, *Chemistry of the Elements* (Butterworth, Washington, D. C., 1984).
[19] A. Filipponi, M. Borowski, D. T. Bowron, S. Ansell, S. De Panfilis, A. Di Cicco, and J. P. Itie, Rev. Sci. Instrum. **71**, 2422 (2000).
[20] A. Filipponi, 1999 *Online available at* http://www.aquila.infn.it/people/Adriano.Filipponi.html/BCD/BCD_tubular_oven.html (July, 2007).
[21] J. A. Solera, J. Garcia, and M. G. Proietti, Phys. Rev. B **51**, 2678 (1995).
[22] A. Kodre, I. Arčon, and R. Frahm, J. Phys. IV **7**, 195 (1997).
[23] A. Kodre, R. Prešeren, I. Arčon, J. Padežnik Gomilšek, and M. Borowski, J. Synchrotron Radiat. **8**, 282 (2001).
[24] B. K. Teo, *EXAFS; Basic Principles and Data Analysis* (Springer-Verlag, Berlin, Heidelberg, 1986).
[25] Nguyen Van Hung and J. J. Rehr, Phys. Rev. B **56**, 43 (1997).
[26] R. J. Magaña and J. S. Lannin, Phys. Rev. B **32**, 3819 (1985).
[27] B. Ravel and M. Newville, J. Synchrotron Radiat. **12**, 537 (2005).
[28] J. J. Rehr and R. C. Albers, Rev. Mod. Phys. **72**, 621 (2000).
[29] A. Filipponi, J. Phys. B **33**, 2835 (2000).
[30] C. M. Teodorescu, R. C. Karnatak, J. M. Esteva, A. El Afif, and J.-P. Connerade, J. Phys. B **26**, 4019 (1993).
[31] C. Froese–Fischer, Comput. Phys. Commun. **43**, 355 (1987).
[32] K. G. Dyall, I. P. Grant, C. T. Johnson, F. A. Parpia, and E. P. Plummer, Comput. Phys. Commun. **55**, 425 (1989).
[33] M. O. Krause and J. H. Oliver, J. Phys. Chem. Ref. Data **8**, 329 (1979).
[34] M. Fritsch, C. C. Kao, K. Hamalainen, O. Gang, E. Forster, and M. Deutsch, Phys. Rev. A **57**, 1686 (1998).
[35] A. Meden, A. Kodre, J. Padežnik Gomilšek, I. Arčon, I. Vilfan, D. Vrbanič, A. Mrzel, and D. Mihailović, Nanotechnology **16**, 1578 (2005).